Available online at www.scholarsresearchlibrary.com

Scholars Research Library

Archives of Applied Science Research, 2013, 5 (4):154-164
(http://scholarsresearchlibrary.com/archive.html)

ISSN 0975-508X
CODEN (USA) AASRC9

Electrical, optical and thermal studies on phase matchable nonlinear optical material

S. Dhanuskodi[1*], A. Philominal[1], J. Philip[2] and J. Yi[3]

[1]*School of Physics, Bharathidasan University, Tiruchirappalli, India*
[2]*Sophisticated Test and Instrumentation Centre, Cochin University of Science and Technology, Cochin, India*
[3]*School of Information and Communication Engineering, Sungkyunkwan University, Chunchun-Dong, Suwon, Korea*

ABSTRACT

A second order nonlinear optical material 1-ethyl-2, 6-dimethyl-4 hydroxy pyridinium zinc sulphate (EDMPZS) was designed and synthesized. The molecular structure was confirmed by FTIR and NMR techniques. Thermal stability was recorded by TG/DTA and DSC. The lower cutoff wavelength (263 nm) and a wide optical transmittance window covering the UV-Visible region were determined by UV-Vis spectra. Single crystals (10 x 2 x 2 mm^3) were grown by solvent evaporation technique at 298 K. Dielectric measurements were carried out using a LCR meter and the electrical parameters viz, dielectric constant (ε') and loss (ε"), real (Z') and imaginary (Z") part of impedance, relaxation time (τ) were evaluated. The powder second harmonic generation (SHG) efficiency was found to be 6.2 times that of KDP and the phase matching property was established.

Keywords: A Optical Materials; B Chemical Synthesis; C Thermogravimetric Analysis; D Electrical Properties
PACS: 76.30

INTRODUCTION

Molecular nonlinear optical (NLO) materials are now being widely investigated for various applications in the field of optical processing such as wide bandwidth electro-optic (EO) modulators, optical switches and frequency convertors [1]. In contrast to inorganics, organic materials possess high nonlinearity and also diversity in molecular and material design [2-3]. It is reported that the ethyl and methyl [4] derivatives of 2, 6 – dimethylamino pyridinone (EDMP, MDMP) exhibit second order NLO effect. However, their thermal, mechanical and chemical stabilities are not high enough to suit device fabrication. The addition of halides (X = Cl, Br) into an EDMP entity leads to the centrosymmetric molecules EDMPCl, EDMPBr [5]. The presence of halides in EDMPX enhances optical transmittance window and the crystal growth habits. The materials based on metal–organic co-ordination networks are therefore advantageous in their transparency / nonlinearity trade off. Thus the co-ordination driven self-assembly provides a unique opportunity to prepare ordered arrays of molecules and clusters of metal – organic frameworks with novel topologies and potentially exploitable functions. The addition of metal may lead to a non - centrosymmetric structure at the molecular level [6-7]. Hence an efficient metal – organic co-ordination compound with improved stabilities was designed. In the present work, the synthesis of a second order NLO material 1-ethyl-2, 6-dimethyl-4 hydroxy pyridinium zinc sulphate (EDMPZS) and its spectral, thermal and optical characterizations are reported.

MATERIALS AND METHODS

2. Synthesis and Crystal Growth

EDMPZS was synthesized by dissolving EDMP [8] and $ZnSO_4$ in equimolar ratio in aqueous solution and the mixture was continuously stirred for 2 hours at 303 K using a magnetic stirrer to ensure homogeneous solution. Then it was evaporated to dryness by heating at 303 K to prevent possible decomposition. Finally a fine crystalline powder of EDMPZS was obtained and it was dissolved in triple distilled water at 303 K to form a saturated solution. This was filtered twice in order to remove the suspended impurities and kept for crystallization by slow evaporation. Transparent needle shaped single crystals of dimensions (10 x 2 x 2 mm^3) at 303 K were harvested within a period of 10 days (**Fig.1**).

3. Spectral, Thermal, Optical and Dielectric Studies

FT-IR spectra were recorded using a JASCO 460 PLUS FT - IR Spectrometer in the range (400 – 4000 cm^{-1}) by KBr pellet technique (**Fig. 2)**. ^1H NMR (300 MHz, D_2O, 300 K) and ^{13}C NMR (300 MHz, $CDCl_3$, 300 K) spectra were recorded using a JEOL Model GSX 400 and Bruker FT-NMR spectrometer respectively (**Figs. 3a and 3b)**. Thermogravimetric / Differential thermal analyses were performed using a Seiko Instruments Thermal Analyzer in the temperature range 28° - 820 °C at a heating rate of 20 °C/min in nitrogen atmosphere. The thermo-gram, with the corresponding percentage of weight shown along the abscissa, is shown in **Fig. 4a**. DSC measurement was carried out using a Mettler Toledo DSC 822^e differential scanning calorimeter in the temperature range 30° - 500 °C at a heating rate of 10 °C/min **(Fig. 4b)**. Optical absorption spectrum was recorded using a Varian Cary 5E UV-Vis Spectrophotometer in the range 200 – 800 nm with the sample dissolved in MeOH solution (**Fig. 5).** Powder second harmonic generation measurements with the particles size (in μm) <106, 106-125, 125-150, and >150 were carried out following the Kurtz-Perry method [9] using a Q-switched Nd: YAG laser (1064 nm, 10 ns, 10 Hz, 3.3 mJ). Dielectric and impedance measurements were carried out using a HIOKI LCR HiTESTER as a function of frequency (42 Hz – 5 MHz) at 303 K.

RESULTS AND DISCUSSION

FT-IR spectroscopy is used to identify the functional groups present in the compound and to confirm the molecular structure [10]. From the spectrum, the H – bonded, O–H stretching frequency is observed at 3382 cm^{-1} whereas EDMP lies in the region of 3390 - 3185 cm^{-1}. The aromatic C–H stretching of first overtone at 1549 cm^{-1} and bending at 1439 cm^{-1} and 1455 cm^{-1} for EDMP and EDMPZS respectively. EDMP shows C ═ O stretching and bending at 1631 cm^{-1} and 494 cm^{-1} whereas for EDMPZS observed at 1627 cm^{-1} and 500 cm^{-1} respectively. The band at 1525 cm^{-1} and 1524 cm^{-1} for EDMP and EDMPZS show the C ═ C stretching. The C–N stretching for EDMPZS and EDMP are noted at 1182 cm^{-1} and 1183 cm^{-1} respectively. The C–H bending deformations are identified at wave numbers 881, 848, 697 cm^{-1} and 875, 852, 731 cm^{-1} for EDMP and EDMPZS respectively. The vibrational frequency at 984 cm^{-1} evidences the presence of SO_4 in the synthesized compound whereas it is absent in EDMP. The position of the other main bands present in both EDMPZS and EDMP are tabulated (**Table-1**).

The proton and carbon configurations of EDMPZS are elucidated by ^1H and ^{13}C NMR spectroscopy [11]. From the ^1H NMR spectrum, the chemical shift at δ = 4.68 ppm denotes the presence of water molecules. The quartet and triplet at δ = 3.95 ppm, and δ = 1.12 ppm are due to the ethyl group. The singlets at δ = 2.26 ppm, and δ = 6.19 ppm are due to the methyl group.

From the ^{13}C NMR spectrum, the peaks at δ = 177.94 ppm and δ = 152.14 ppm indicate the carbonyl group (C ═ O) attached to the aromatic ring. The signals at δ = 13.38 ppm and δ = 19.38 ppm address the presence of ethyl group and the shift at δ = 116.86 ppm denotes the presence of olefinic hydrogen (C – H).

Thermal stability of the compound was determined through TG/DTA and DSC thermo-grams. The initial mass of the material taken for the analysis was 6.321 mg. From the TGA curve, the weight loss was observed in the temperature region 38 ˚- 110 ˚C due to the water molecules in the surface of the lattice. An endothermic peak at 283.48 ˚C is identified as due to melting of the material whereas EDMP melts at 165 ±1 °C. An endothermic peak observed in the region 300˚- 500 ˚C reveals the decomposition of the compound whereas TGA shows a complete weight loss and the residual weight observed at 800 ˚C was only 5% of the initial mass. Also the melting point and the decomposition temperature of the compound were confirmed through DSC analysis.

From the optical absorption spectrum, it is evident that the material has a good optical transmittance window (263 – 800 nm) and the lower cutoff wavelength at 263 nm qualifies it for the generation of higher harmonics of Nd: YAG laser in the UV region.

The SHG outputs for EDMPZS, EDMP, KDP are 295, 56 and 61 mV respectively for the particle size range of >150 µm (**Table-2)**. The plot of SHG output vs particle size is shown in **Fig. 6**. EDMPZS shows the relative powder SHG efficiency is 5.4 times of EDMP and 6.2 times that of KDP. The increase in SHG efficiency for EDMPZS compared to the parent molecule EDMP is attributed to the presence of metal ion. The measurement of SHG output for various particle size ranges shows the increasing SHG intensities with increasing particle size, which confirms the phase matching behaviour of the material.

Impedance spectroscopy is a powerful technique for the measurement of electrical properties of materials over a suitable frequency range. It provides frequency resolved information which can detach the contributions of different component regions (bulk, material/contact and interface) to the total electrical properties of devices through differences in the time constants of each element viz, the series resistance Rs (due to bulk and contact resistances), the parallel resistance R_p (due to recombination in the depletion region) and total capacitance C_0 (sum of diffusion and depletion capacitances) [13-17].

Polycrystalline sample of EDMPZS was made in the form of pellet with a thickness of 1.1 mm and the dielectric and impedance measurements were carried out using a HIOKI LCR meter in the frequency range 42 Hz –5 MHz at 303 K. The opposite flat faces of the pellet were coated with conducting silver paint to form a parallel plate capacitor. The capacitance of the parallel plate capacitor (C), impedance (Z), phase angle (θ) and dissipation factor (D) were measured.

4.1 Electrical conductivity studies

Electrical conduction takes place as a result of electron jumping from the of low valence state to high valence state of the metal ion as well as the movement of ions. The dc electrical conductivity can be calculated using the relation

$$\sigma_{dc} = \frac{d}{AR_{dc}} \qquad \text{---------- (1)}$$

Where R_{dc} is the total electrical resistance of the sample and it is evaluated from the Cole - Cole plot (or Nyquist diagram) by plotting Z' (real part of impedance) against Z" (imaginary part of impedance) (**Fig 7**). The equivalent circuit containing Rp, Rs, and Co describes the electrical response of the systems with a single relaxation frequency. It shows a depressed semicircle at high frequency and a linear branch at low frequency that describes the electrode polarization. The electrical parameters of EDMP and EDMPZS are shown in table-3. It can be seen that the low value of dc conductivity is due to the decreases in mobility of the charge carriers by ion size which bring the prominent changes in the electronic band structure. This plot is also applicable for the study of Debye relaxation in materials. It shows a semicircle, and will be useful in describing Debye relaxation for materials possessing large dc conductivity. By knowing the radius of the semicircle, the magnitude of relaxation time can be evaluated. If the radius is greater, lesser the relaxation time and hence at higher frequencies it can be reduced due to the enlargement of the semicircle. The relaxation times were calculated from the frequency at which Z" maxima were observed using the following relation,

$$\omega\tau = 1 \text{ or } \tau = 1/\omega \qquad \text{---------- (2)}$$

Where ω is the relaxation frequency and τ is the relaxation time.

The measurements of real and imaginary parts of the complex impedance is represented as $Z^* = Z' + jZ''$ [$\because j = (-1)^{1/2}$], where Z' = Re Z= |Z| cosθ, Z"=|Z| sinθ. The corresponding complex resistivity of the material is $\rho^*=\rho' - j\rho''$ where $\rho'= Z'A/d$ and $\rho''= Z''A/d$, A and d are the cross-sectional area and thickness of the sample. The complex conductivity is $\sigma^*=1/\rho^*=\sigma' - j\sigma''$ where $\sigma' = \rho'/M$ and $\sigma'' = \rho''/M$ with the electric modulus $M = |Z^*|^2 (A/d)^2$. **Fig. 8(a) and (b)** show the variation of real (Z') and imaginary (Z") part of impedance with log frequency at 303 K. It

can be seen that the curve displays a decrease in Z' with frequency. The Z" values reach a maximum with increasing frequency and shift to lower frequencies indicates decreasing relaxation time. This behavior of impedance pattern arises due to the presence of space charge in the material. Plots of Z' vs Z" for the range of frequencies show semicircular nature indicating the predominance of a single time constant.

Plots of ε'and ε" against *log (frequency)* at 303 K is shown in **Fig. 9(a) and (b)**. It is observed that, the dielectric constant and loss decrease with increase in frequency and the high dielectric constant at low frequencies is due to the space charge polarization. Because of the inertia of the molecules at high frequencies, the orientation and ionic contribution of polarization are small. Hence the magnitude of polarization increases with decrease in frequency. The lowest value of dielectric constant of EDMPZS is found to be 4 at 5 MHz.

4.2 Electric modulus

The electrical relaxation has been extensively studied and analyzed in terms of modulus formalism [18]. The advantage is that the electrode polarization effects are suppressed in this representation. The real (σ') part of the conductivity is related to the electrical modulus and can be expressed following the equation

$$\sigma'(\omega) = \omega\varepsilon_0\varepsilon''(\omega) = \omega\varepsilon_0 \frac{M''(\omega)}{|M^*(\omega)|^2} \qquad \text{---------- (3)}$$

Where *M"* is the imaginary part of the complex electrical modulus, M* and |M*| is the magnitude of the modulus. The electrical modulus is defined as the electric analogue of the dynamical mechanical modulus and is related to the inverse of the complex permittivity ε*(ω) by,

$$M^*(\omega) = \frac{1}{\varepsilon^*(\omega)} = \{\varepsilon'(\omega) - i\varepsilon''(\omega)\}|\varepsilon^*(\omega)|^2 = M'(\omega) + iM''(\omega) \qquad \text{---------- (4)}$$

Where *M'(ω)* and *M"(ω)* are the real and imaginary parts of the electric modulus. The modulus spectra of EDMPZS in **fig. 9 (c) and (d)** show the electrical relaxation with a peak frequency in the imaginary part of the modulus spectra M". In the present case, it is observed that the interaction among the dipoles increases and hence the relaxation becomes slower, reducing the relaxation frequency. Thus the studies were performed to understand the electrical properties by means of impedance spectroscopy, the frequency response of the material under an alternating current was studied.

Table 1: Comparison of FTIR vibrational frequencies of EDMPZS with EDMP

Wavenumber (cm^{-1})		Assignments
EDMP [12]	EDMPZS	
3390-3185	3382	υ (O−H), H-bonded
3000	-	υ (C−H)
1631	1627	υ (C═O)
1549	1548	υ (C−H), overtone
1525	1524	υ (C═C)
1455	1439	δ (C−H)
1375, 1338	1379, 1338	δ (C−H of CH_3)
1198, 1183	1182, 1139	υ (C−N) or ρ(C−H)
1034	-	υ (C−N)
-	984	υ_s (SO_4)
881, 848	875, 852	π (C−H)
697	731	π (C−H)
-	619	δ (O−H)
494	500	π (C═O)

υ - stretching, υ_s - symmetric stretching, δ - bending deformation in plane, ρ - rocking in plane, π - bending out of plane

Table-2: Comparison of SHG output for various particle size ranges

Particle size (μm)	SHG output (mV)		
	KDP	EDMP [12]	EDMPZS
<106	16	33	150
106-125	25	36	190
125-150	43	49	255
>150	61	56	295

Table-3: Electrical parameters of EDMPZS and EDMP at room temperature (303 K)

System	R_{dc} (Ωm)	σ_{dc} (10^{-5} mho m^{-1})	C_{dc} (10^{-7}f)	Depression angle θ	Relaxation frequency ω_p (KHz)	Relaxation time τ(s)
EDMP	89098	9.3040	3.4480	11.158	31.936	0.035
EDMPZS	2.0506×10^5	4.0424	1.3997	42.753	25.582	0.039

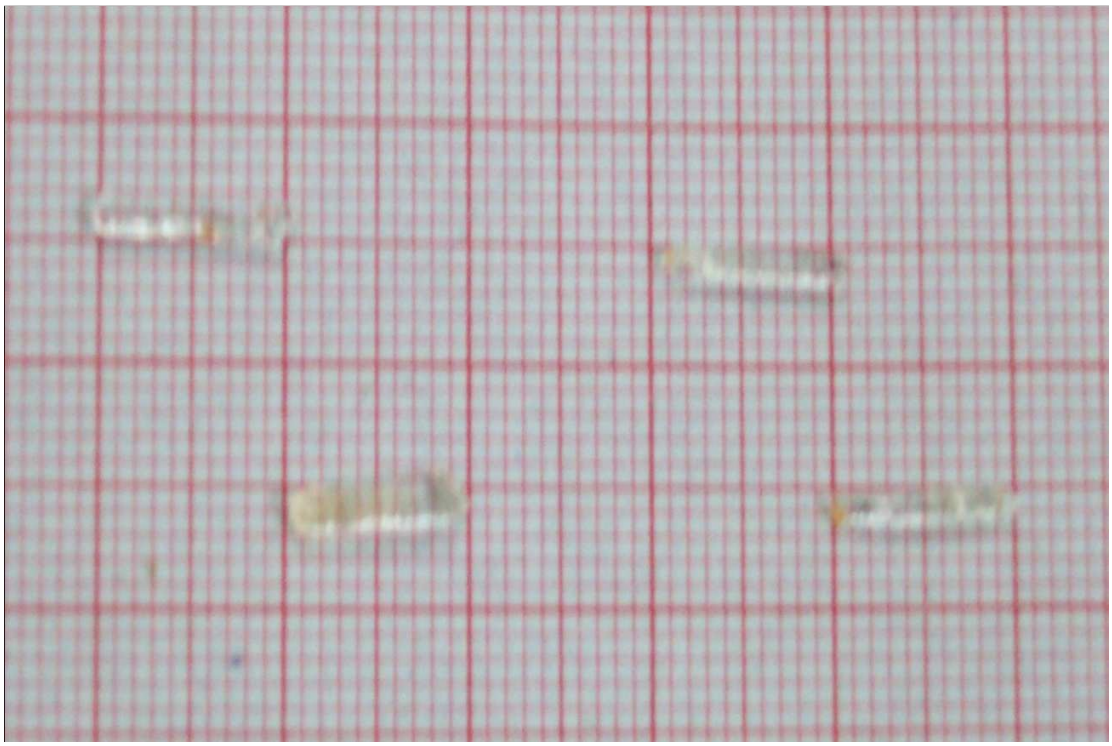

Fig. 1: Grown single crystals of EDMPZS

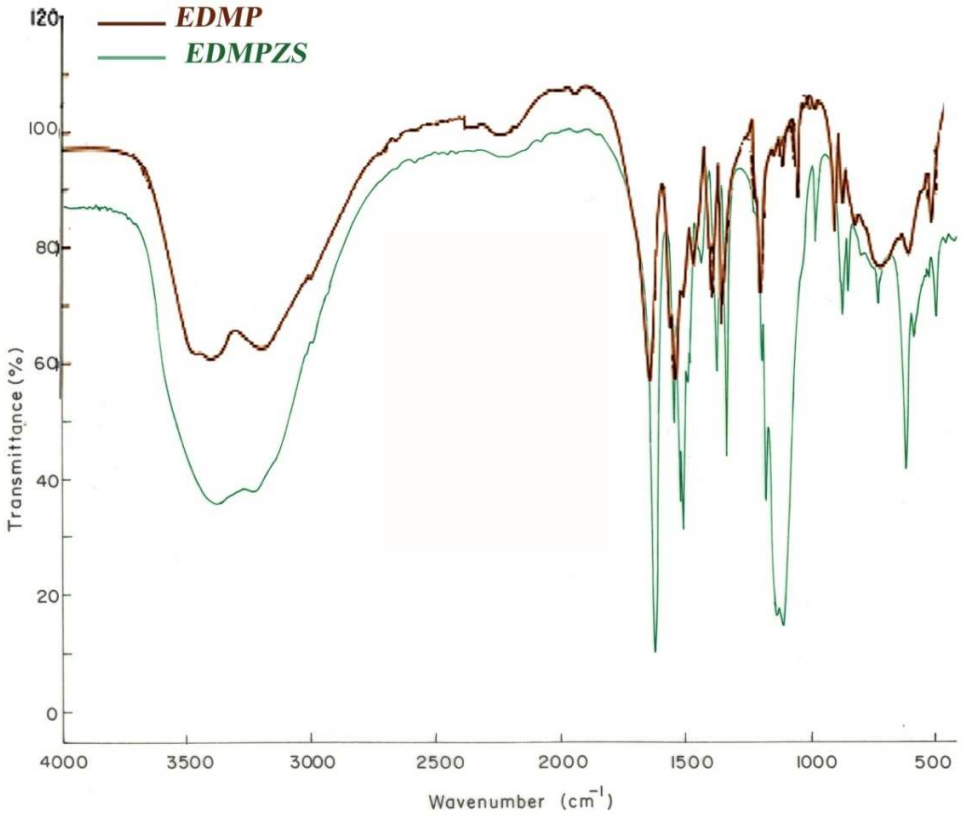

Fig. 2: FT-IR overlay spectrum of EDMPZS with EDMP

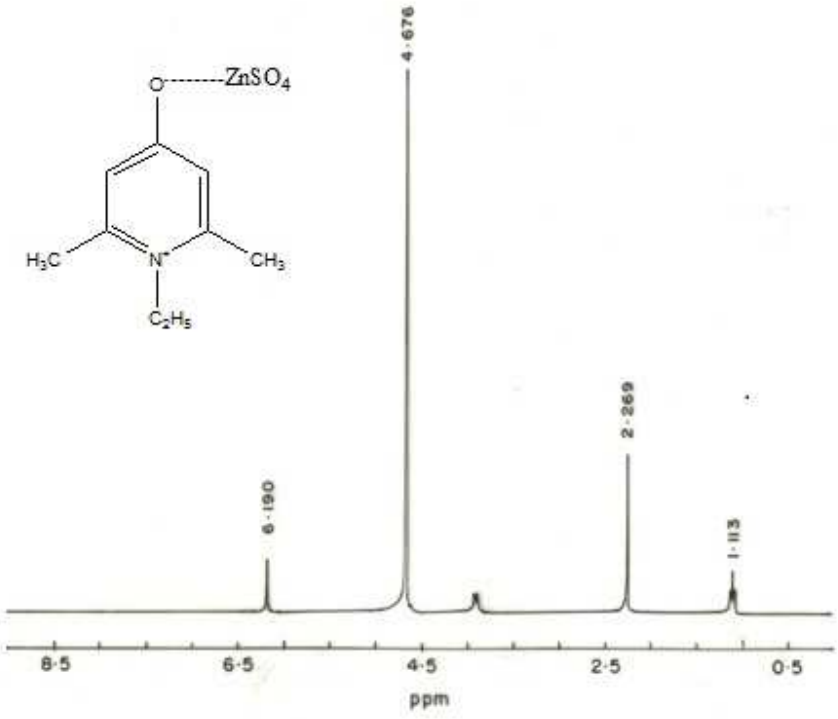

Fig. 3a: ^{1}H NMR spectrum of EDMPZS

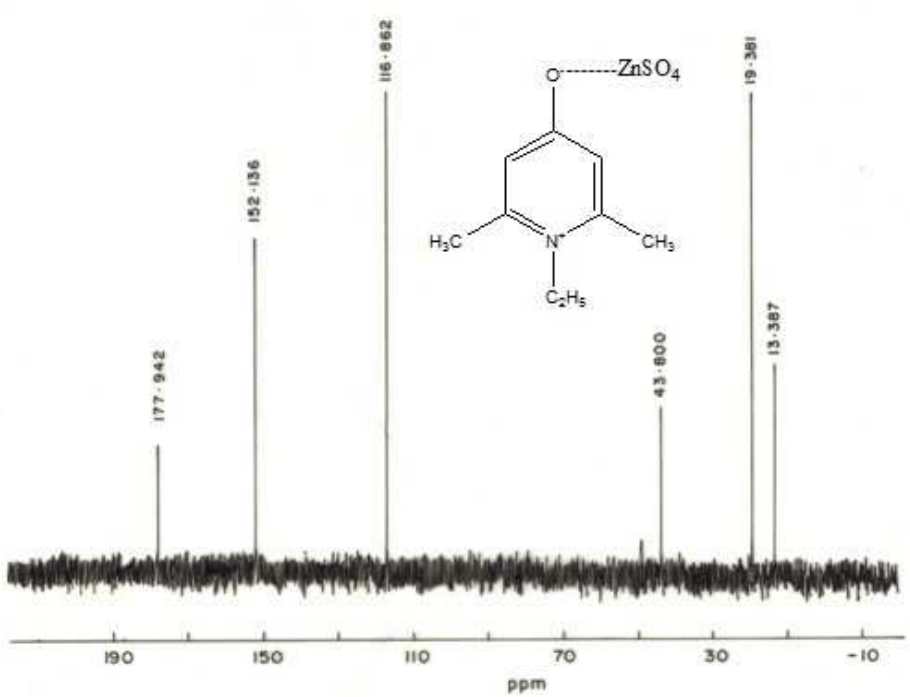

Fig. 3b: ^{13}C NMR spectrum of EDMPZS

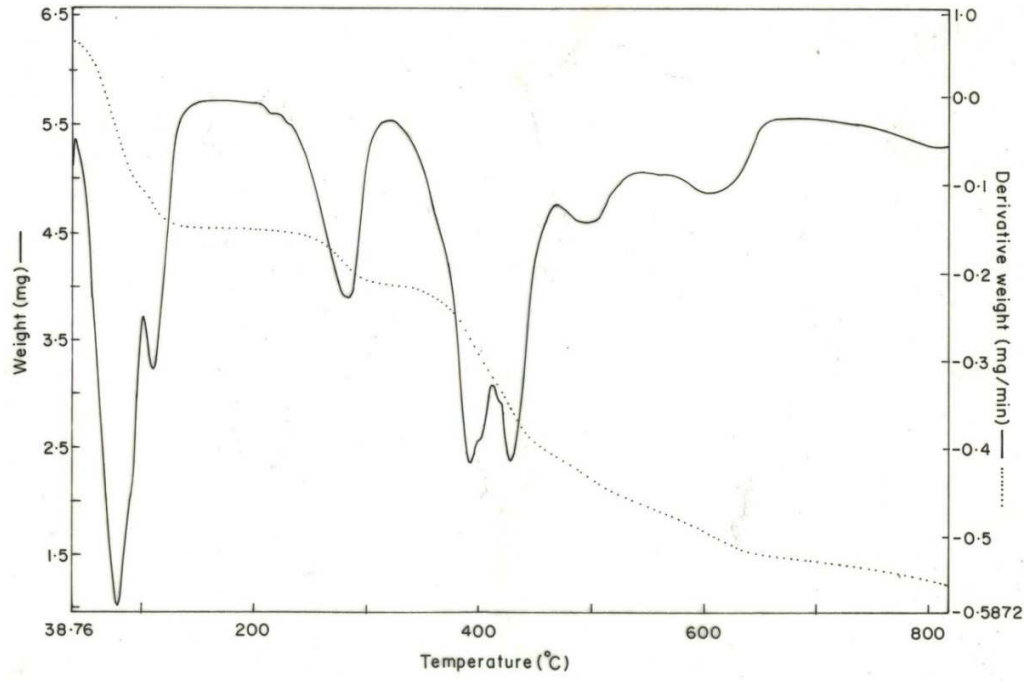

Fig. 4a: TG/DTA curves of EDMPZS

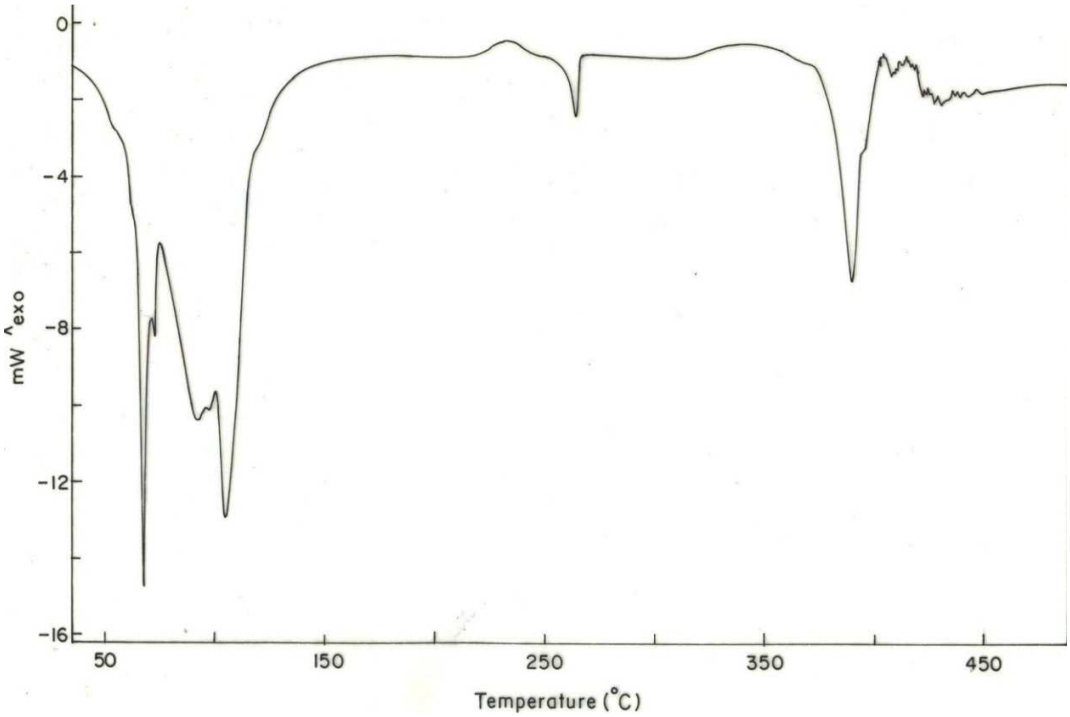

Fig. 4b: DSC curve of EDMPZS

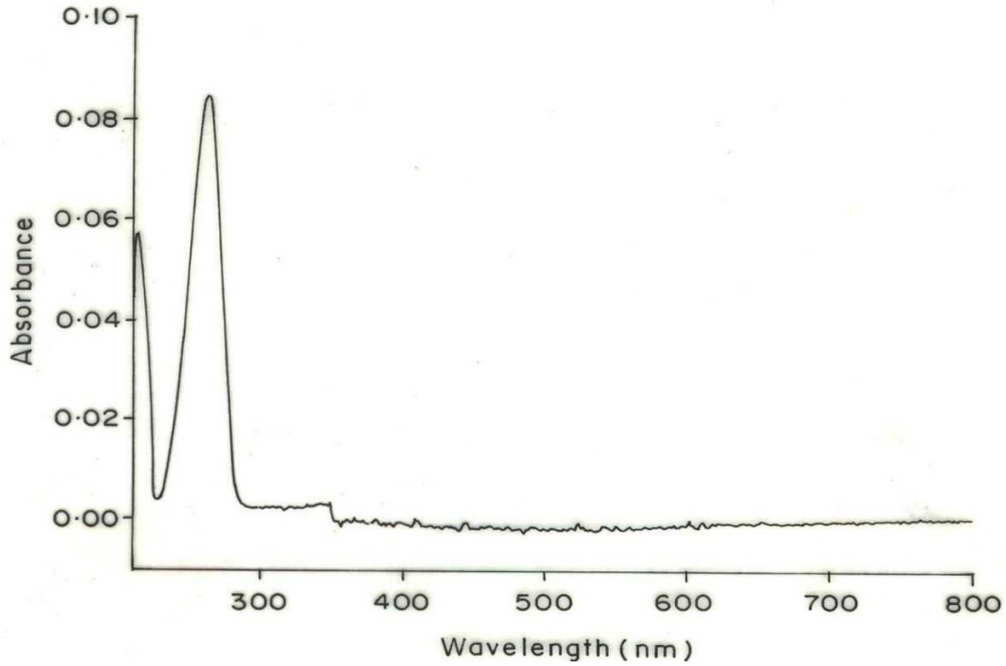

Fig. 5: UV – Vis Absorption spectrum of EDMPZS

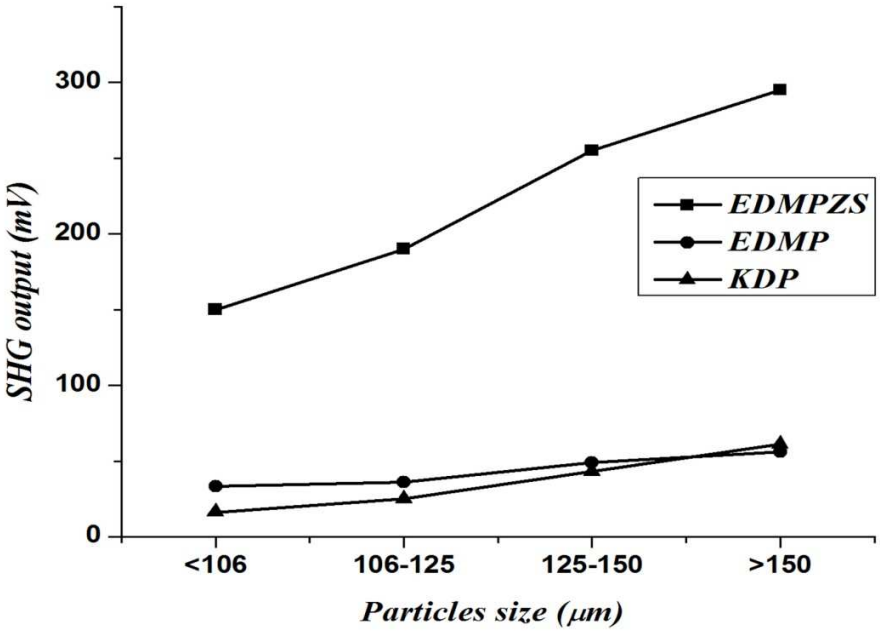

Fig. 6: Variation of SHG output with Particle size

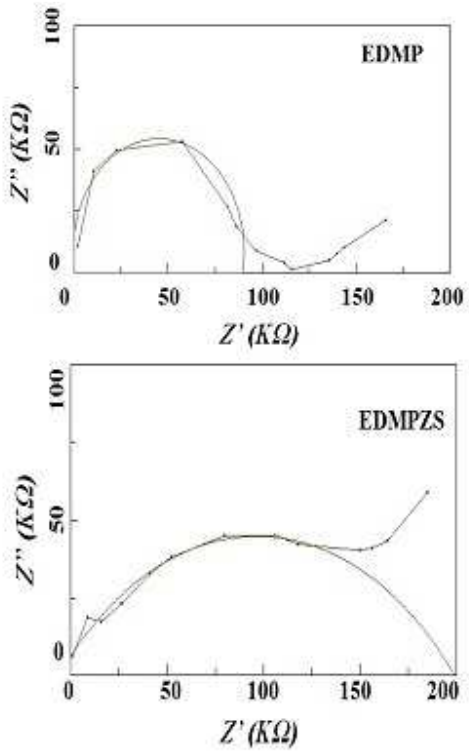

Fig. 7: Complex plane or Nyquist plot of EDMPZS and EDMP

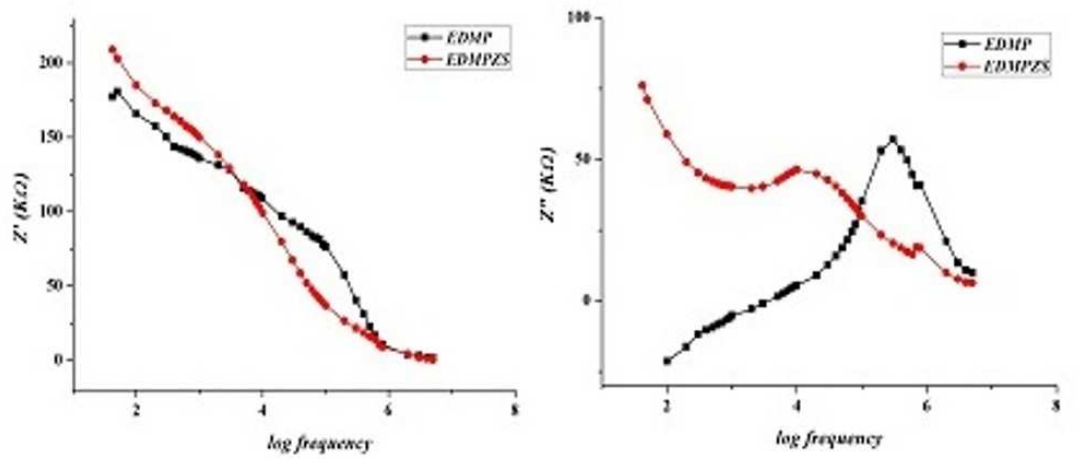

Fig. 8: Variation of (a) real part of the impedance (b) imaginary part of the impedance against log frequency at 303 K for EDMPZS and EDMP

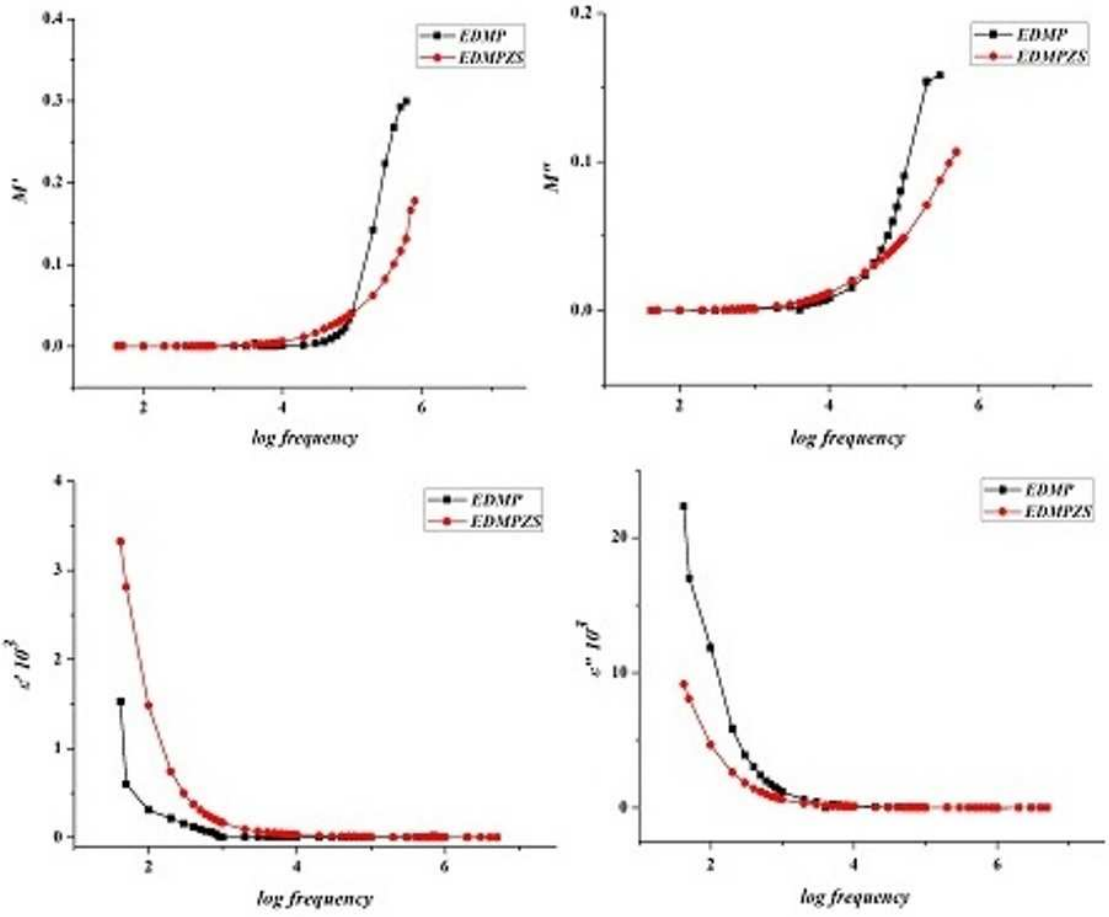

Fig. 9: Variation of (a) real part of dielectric constant (b) imaginary part of dielectric constant (c) real part of electric modulus and (d) imaginary part of electric modulus against log frequency at 303 K for EDMPZS and EDMP.

CONCLUSION

A novel second order nonlinear optical material 1-ethyl-2, 6-dimethyl-4-hydroxy pyridinium zinc sulphate was designed, synthesized and single crystals were grown by solvent evaporation technique. The molecular structure was confirmed by FT-IR and FT-NMR spectroscopy. The thermal stability was determined from the TG/DTA and DSC curves. From the impedance studies, the lowest value of the dielectric constant is found to be 4 at 5 MHz and the relaxation time is 10 µs. The analysis of the complex impedance data through a complex – plane impedance representation and the evaluation of the dielectric permittivities provide more insights into the dielectric behavior of the materials. The relaxation due to the interfacial and orientational polarization is the main factors that affect their dielectric behavior. Atomic and electronic polarization may only contribute a small constant term to the dielectric constant since the structural frequencies for atomic and electronic displacements and relaxation are in the microwave regime. The optical absorption spectrum reveals that the lower cutoff wavelength is at 263 nm and a wide optical transmittance window in the region (263 – 800 nm) makes this material a good candidate for the generation of higher harmonics in the UV region. SHG measurements show that the material satisfies the phase matching properties and so is a promising material for nonlinear optical applications.

Acknowledgements
The authors thank Prof. K. Panchanatheeswaran, Department of Chemistry, Bharathidasan University, Tiruchirappalli, India for fruitful discussions. The authors acknowledge the help of Prof. P. K. Das, Department of Inorganic and Physical Chemistry, Indian Institute of Science, Bangalore for SHG measurements. This work is supported by the Ministry of Information and Communication, Korea, under the ITPSIP (IT Foreign Specialist Inviting Program) supervised by the IIT A (Institute of Information Technology Advancement).

REFERENCES

[1] I. C. Khoo, F. Simoni, C. Umeton, Novel Optical Materials and Applications, John. Wiley & Sons Inc, **1997**.
[2] M. S. Wong, J. F. Nicoud, C. Runser, A. Fort, M. Barzoukas, *Nonlinear Opt*., **1995**, 9 181.
[3] V. D. Costa, J. L. Moigne, L. Oswald, T. A. Pham, A. Theirry, *Macro Molecules*, **1998**, 31, 1635-1643.
[4] S. Garratt, *J. Org. Chem*., **1963**, 28, 1886-1888.
[5] S. Dhanuskodi, S. Manivannan, J. Philip, *J. Cryst. Growth*, **2005,** 265, 284-289.
[6] Owens R. Evans W. Lin, *Acc. Chem. Res*., **2002,** 35, 511-522.
[7] X.X. Zhao J. P. Ma, Y. B. Dong, R. Q. Huang, *Crystal Growth & Design*, **2007**, 7, 1058-1068.
[8] Y. L. Fur, R. Masse, M. Z. Cherkaoui, J-F. Nicoud, *Z. fur Kristallographie*, **1995,** 210, 856-860.
[9] S. K. Kurtz, T. T. Perry, *J. Appl. Phys*., **1968, 39,** 3798-3813.
[10] R. M. Silverstein, F. X. Webster, Spectroscopic Identification of Organic Compounds (John Wiley & Sons (Asia) Pvt. Ltd., **2003**, 6th Edn.
[11] P. S. Kalsi, Spectroscopy of Organic Compounds (New Age International (P) Ltd., New Delhi, **2002**, 5th Edn.
[12] S. Manivannan, S. K. Tiwari, S. Dhanuskodi, *Solid State Commun*., **2004**, 132, 123-127.
[13] R. A. Kumar, M. S. Suresh, J. Nagaraju, *Sol. Energy Mats. Sol. Cells*, **2000**, 60 155-166.
[14] Habibe Bayhan, A. Sertap Kavasoglu, *Turk J. Phys*., **2003**, 27, 529-535.
[15] A. K. Jonscher, Dielectric Relaxation in Solids, Chelsea Dielectrics Press, London, **1983**.
[16] R. Rizwana, T. Radha Krishna, A. R. James, P. Sarah, *Cryst. Res. Technol*., **2007**, 42, 699-706.
[17] S. Suresh, A. Ramanand, P. Mani, K. Anand, Scholar Research Library: *Archives of Applied Science Research*, **2010**, 2, 119-127.
[18] N. Ponpandian, P. Balaya, A. Narayanasamy, *J. Phys.: Condens. Matter*, **2002**, 14, 3221-3237.